16th International Conference on Space Operations, Cape Town, South Africa – 3 - 5 May 2021.

SpaceOps-2021, 7, x1512

In-orbit fragmentations localisation: study and characterisation of the events

Andrea Muciaccia[a]*, Matteo Romano[a], Camilla Colombo[a], Mirko Trisolini[a]

[a] *Department of Aerospace Science and Technology (DAER), Politecnico di Milano, Via Giuseppe La Masa 34, 20156, Milano, Italy, Email:*
{matteo1.romano, andrea.muciaccia, camilla.colombo, mirko.trisolini}@polimi.it
* Corresponding Author

Abstract

The number of breakup events (i.e., collisions and explosions) is growing in recent years, resulting in an increase in the number of uncontrollable objects orbiting around the Earth. Despite the presence of debris mitigation guidelines, defined to manage satellites during their entire lifetime, some events are still difficult to predict or even unpredictable. Is also well known that some orbital regions have higher risks for collisions to happens and unforeseen breakup events can occur due to system failures. The knowledge and the characterisation of fragmentations is necessary to ensure the safety of the satellites already in orbit and of those that will be launched in the future.

The proposed work has two main goals: the detection of possible occurred fragmentation events and the identification of the probable parent(s) that originated the fragments. The search is carried out considering a time frame, for the event detection, in the range of months up to years, and adopting mean Keplerian orbital elements to study the evolution in time of all the analysed objects. The current study focuses on the low Earth orbit region, taking advantage of its characteristics (e.g., the evolution in time of some orbital elements like the orbit inclination and right ascension of the ascending node). Different tools are included in the developed models: an outlier filter to handle possible errors detected in the input set of data (i.e., the Two-Line-Elements (TLEs)), an algorithm to estimate the ballistic coefficient of each object from the data included in the TLEs, and pruning and clustering techniques for the identification of fragments belonging to different families (i.e., different parent object(s)). Tests are performed to validate the models to satisfy both the goals, considering set of objects composed by a single family (i.e., debris belonging to the same parent) or by different families (i.e., debris belonging to different parents).

Keywords: Space debris, in-orbit fragmentations, low Earth orbit, space debris.

Nomenclature

a	Semi-major axis [km]
a_{TLE}	Semi-major axis included in the TLE [km]
a	Semi-major axis [km]
D_{th}	Threshold distance [km]
i	Orbit inclination [deg]
n	Mean motion [rev/day]
n_{reg}	Mean motion evaluated by the regression algorithm
q	Perigee distance [km]
Q	Apogee distance [km]
r_f	Distance of the first body [km]
$\dot{r}_f$	Derivative of the distance of the first body[km/s]
$\ddot{r}_f$	Second derivative of the distance of the first body[km/s^2]
$\boldsymbol{r_f}$	First body position vector [km]
$\dot{\boldsymbol{r}}_{\boldsymbol{f}}$	Derivative of the position vector of the first body [km/s]

$\ddot{\boldsymbol{r}}_{\boldsymbol{f}}$	Second derivative of the position vector of the first body [km/s^2]
r_s	Distance of the second body [km]
$\dot{r}_s$	Derivative of the distance of the second body[km/s]
$\ddot{r}_s$	Second derivative of the distance of the second body[km/s^2]
$\boldsymbol{r}_s$	Second body position vector [km]
$\dot{\boldsymbol{r}}_s$	Derivative of the position vector of the second body [km/s]
$\ddot{\boldsymbol{r}}_s$	Second derivative of the position vector of the second body [km/s^2]
R_{rel}	Rate of change of the relative distance between two objects
$\dot{R}_{rel}$	Derivative in time of R_{rel}
t	Time [day]
t_{estim}	Estimated date of the event [day]
t_{last}	Initial date of the analysis [day]
t_{real}	Real date of the event [day]
ε_{rell}	Relative error
μ_E	Earth gravitational parameter [m^3/s^2]
Ω	Right ascension of ascending node [deg]
Ω_0	Right ascension of ascending node computed through the propagator [deg]
$\dot{\Omega}$	Derivative in time of the right ascension of ascending node [deg/s]

Acronyms/Abbreviations

BC	Ballistic coefficient
GEO	Geostationary Earth Orbit
HCM	Hierarchical Clustering Method
HEO	Highly Elliptical Orbit
LEO	Low Earth Orbit
MAD	Mean Absolute Deviation
MEO	Medium Earth orbit
MOID	Minimum Orbit Intersection Distance
NASA	National Aeronautics and Space Administration
PlanODyn	Planetary Orbital Dynamics
RAAN	Right ascension of ascending node
SOFT	Simulation of On-Orbit Fragmentation Tool
TLE	Two Line Element

1. Introduction

Fragmentation reconstruction and characterisation is fundamental for future space traffic management and operation of new missions and those already in orbit. The amount of uncontrollable space objects is constantly increasing, and the current number for the Low Earth Orbit (LEO) region is of around 9700 debris out of a total of 13930 orbiting catalogued objects as of end of 2019 [1]. The increase in the space pollution results in some orbital regions to be at higher risk of breakup events. Despite the presence of guidelines, some breakup events are still difficult to be avoided (e.g., collisions between objects in space), while others are hardly predictable (e.g., explosion of rocket bodies). Building the capabilities to properly localise and characterise fragmentations could lead to an improvement for mission design and operations. Fragmentation reconstruction has been treated in different ways in past works, considering various techniques for studying the evolution of the orbital elements, useful for identifying the location and time of occurred breakup events. Andrisan et al. [2] developed the Simulation of On-Orbit Fragmentation Tool (SOFT) to determine the type of fragmentation and the objects involved in it, whenever a space surveillance network detects unexpected new objects. The type of fragmentation (i.e.,

explosion or collision) is defined looking at the distribution of the orbital parameters of the detected new objects. The location and the date of the events is searched by propagating backward the fragments and by checking the average distance between them, looking for a possible minimum. The position and the velocity of the of the centre of mass of the fragments, at the event epoch, are used to identify the parent object(s). Romano et al. [3] proposed a method implemented in the software PUZZLE based on osculating orbital elements and a time frame for the event detection up to one month. Their work has two objectives: the detection in space and time of the fragmentations, and the modelling of the distribution of the generated fragments, starting from the identification of the possible parent(s). Pruning and clustering algorithms, that are the triple-loop proposed by Hoots et al. [4] and the Hierarchical Clustering Method (HCM) [5], are exploited to reject wrong fragments, to subdivide the analysed objects into families and to find possible close approaches between the fragments' locations. The NASA standard breakup model is used to recover the physical properties of the fragments and to model the distribution of the orbital parameter of all the possible generated fragments. Dimare et al. [6] attempted to identify the fragmentation epoch and the corresponding parent object(s) with the use of a similarity function based on the orbital elements of the analysed fragments. The latter, all generated by the investigated breakup event, are propagated backward finding the minimum in the similarity function among them. The orbital parameters of the debris at the detected event date are matched with a set of possible candidates to guesses the possible parent(s). Different metrics for the similarity function have been tested: the nodal distance, the Minimum Orbital Intersection Distance (MOID), and the D-criterion (which is a method developed for the study of asteroids' families) proposed by Southworth and Hawkins [7], by Jopek [8], and by Drummond [9]**.** Southworth-Hawkins and Jopek's metrics proved to be the most suitable for achieving both the goals. The method by Frey et al. [10], instead, scans a time frame of the order of months to years to find the event epoch. They identified the inclination and the Right Ascension of Ascending Node (RAAN) as the most suitable orbital elements for the detection of the event date. The proposed idea is to search possible clustering in time of these two Keplerian orbital elements when the fragments are propagated backward. The propagation is performed considering mean orbital elements, making the study different from the previously analysed methods. Moreover, they suggest the use of supervised learning algorithms to train the method.

The work presented is a continuation of the work in [10] and has a twofold objective: first, the detection of occurred fragmentation events (i.e., collisions or explosions); second, the identification of the possible parent object(s) that originated the fragments. As for the method by Frey et al. [10], the time span considered for the study is of the order of months to years (i.e., the long-term evolution of orbits.), and mean Keplerian elements are used for the propagation. All the analyses carried out for the development of the model and for its validation consider Two-Line-Elements (TLEs), publicly available data generally used to perform orbital analysis whenever more accurate orbital data are not available, as data set. The models include different tools: an outlier filter to reject possible errors in the set of TLEs, a routine for estimating the Ballistic Coefficient (BC) that fits the B* parameter included in the TLEs, and pruning and clustering techniques capable of differentiating the examined objects into different families. The analysed objects are propagated backward, exploiting the semi-analytic propagator PlanODyn [11], and the orbital elements are investigated to detect possible convergence and hence possible fragmentation events. The fragments that remain at the end of the process are used to identify the parent object(s), considering as possible candidates known objects included in online catalogues. Figure 1 shows the block diagram of the model.

The paper describes the data pre-processing in Section [0], the model of the event detection in Section [3], and the model of the parent identification in Section [4]. Section [5] is devoted to the presentation of some tests, while Section [6] reports the final considerations and possible future improvements of the method.

Figure 1. Model block diagram.

2. Data pre-processing

Before starting with the fragmentation's analyses, the input data must be organised. TLEs, that are publicly available data generally used to perform orbital mechanics analysis whenever more accurate orbital data are not available, are selected for the investigations. The pre-processing phase takes as input the TLEs data, extracts from them the needed information (e.g., the orbital parameters), filters out possible errors included in the TLEs sequences, and estimates some parameters that are required during the next phases of the process.

2.1 Outlier filtering

The implementation of an outlier filter is necessary to remove from the sequences possible erroneous TLEs and, consequently, to improve the quality of the input data and of all the following analyses. The filter used for the work is the one proposed by Lidtke et al. [12] and, for each sequence of TLEs (corresponding to each considered object), the data are examined through five steps:

1. Check for possible high frequency update time of the TLEs; in these cases, according to a selected threshold, it is possible to consider the new TLE as a correction of the previous one, that hence must be eliminated;
2. Check for possible low frequency update; in the presence of large time gaps, it is necessary to create windows inside which the following filters will be performed;
3. Remove TLEs incoherent values for the mean motion parameter and creation of possible sub-windows;
4. Remove TLEs incoherent values for the inclination and eccentricity parameters;
5. Remove TLEs which include negative values of the B*.

After the elimination of all the TLEs rectified by new TLE update, and the generation of the windows, the mean motion outliers are detected using a sliding window process; the latter is characterised by a fixed length. Inside each window, it is evaluated the polynomial $n_{reg}(t)$ through a regression technique, considering a polynomial of a chosen order. With the obtained regressed polynomial, the two TLEs that follow the window are analysed using two tolerances. The first is an absolute tolerance computed as

$$T_A = \frac{n_i - n_{reg}(t_{i+1})}{n_{reg}(t_i)} \qquad (1)$$

where n_i is the elements $i-th$ in the sliding window, $n_{reg}(t_i)$ and $n_{reg}(t_{i+1})$ are the mean motion evaluated through the regression technique of the $i-th$ and $(i+1)-th$ elements. The second is a relative tolerance computed as

$$T_R = \frac{n_i - n_{reg}(t_i+1)}{n_{reg}(t_i) - n_{reg}(t_i+1)} \qquad (2)$$

In case both the thresholds are exceeded, it is not possible to correctly state whether the analysed element is an outlier or not. Indeed, it is possible that the analysed element is the beginning parameter of a new evolution in the mean motion. Consequently, it is implemented a new tolerance, that is computed as

$$T_{A_{i+1}} = \frac{n_{i+2} - n_{i+1}}{n_{reg}(t_{i+1})} \qquad (3)$$

If also this last threshold is exceeded, the TLE is rejected by the process; contrary, if the new value stays below the threshold, the TLE remain in the process and a new sub-window is generated. The inclination and the eccentricity (considering the perigee radius for the study) are analysed within the previously generated sub-windows. This time, a simpler statistical approach is performed. First of all, a window with a fixed length scans the TLEs sequence and compute the mean value. The latter is subtracted to the TLE in the middle of the window to generate a time series of differences. The time series is scanned by a new window (with a different length) and the Mean Absolute Deviation (MAD) is evaluated. All the elements that present a difference from the mean value that is greater than a chosen number of MAD are eliminated by the process. More than one passage, considering different values for the length of the

windows and for the tolerances, can be performed to reject the outliers at different levels. The last filter performs a simple sign check to eliminate possible negative *B** values. The latter are typically associated to satellite manoeuvres, not considered in these analyses, and possible uncertainty included in this parameter. Figure 2 summarises the steps of the outlier filtering routine.

.

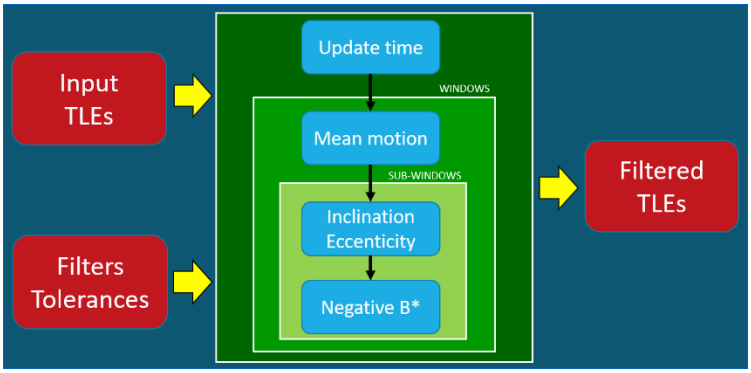

Figure 2. Outlier filter block diagram.

2.2 Ballistic coefficient estimation

The ballistic coefficient is an important physical property of each object and must be estimated to recover a precise time evolution of the objects with the adopted propagator [11]. For this work, it is exploited the method proposed by Gondelach et al. [13]**;** this method was also applied to re-entry prediction by Frey et al [14].The estimation is performed considering as fitting parameter the *B**, that is the drag parameter included in the TLEs and it is used through simplified perturbation propagators [15]. The basic idea of the model is that the change in the semi-major axis (included in the TLEs in terms of mean motion) is related to the drag perturbation only. Figure 3 shows the steps performed to estimate the ballistic coefficient. First, the semi-major axis is recovered from the mean motion included in the TLEs as

$$a = \left(\frac{\mu_E * 86400^2}{\pi^2 n_0^2}\right)^{1/3} \qquad (4)$$

Then, it is computed the change in the semi-major axis between two selected TLEs as

$$\Delta a_{TLE} = a_{TLE_2} - a_{TLE_1} \qquad (5)$$

The same change is performed using the propagator and considering a time interval for the propagation equal to that of the selected TLEs. It is important to state that the propagation is performed backward to avoid possible undesired re-entries of the considered objects. The second change in the semi-major axis, evaluated considering each time the last BC guess, is computed as

$$\Delta a_{prop} = \int_{t1}^{t2} \frac{da}{dt}\Big|_{drag} dt \qquad (6)$$

The change obtained between the TLEs and through the propagator are compared and the process is repeated until the difference between the two values goes below the threshold set at 10^{-4} km [13]. In case the threshold is not satisfied, a new BC guess is generated using a simple secant method

$$BC_n = BC_{n-1} - \Delta a_{diff}(BC_{n-1}) \frac{BC_{n-1} - BC_{n-2}}{\Delta a_{diff}(BC_{n-1}) - \Delta a_{diff}(BC_{n-2})} \qquad (7)$$

For the purpose of this work, the estimation is performed by considering a sinusoidal model to recover the evolution of the solar activity over time; this decision introduces possible uncertainties both in the estimation process and in the propagation one. However, it is necessary to perform a compromise between the accuracy of the model and the computational time of the process.

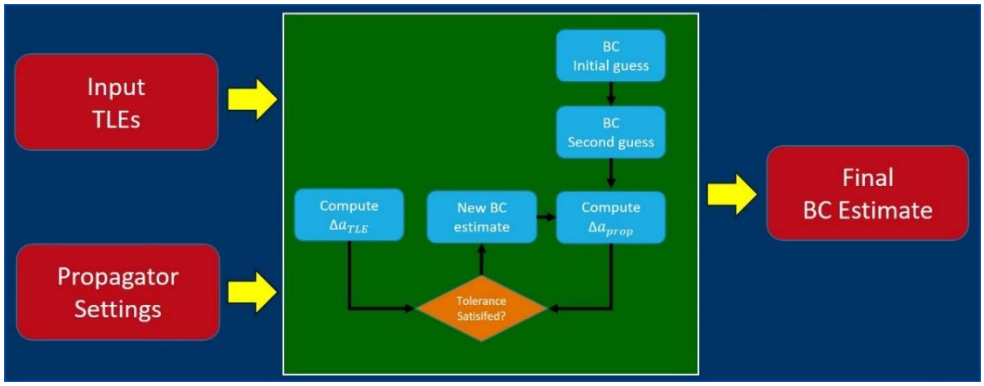

Figure 3. Ballistic coefficient estimation process.

3. Event detection

The first goal of the work is the detection of possible occurred breakup events. According to the composition of the initial set of analysed objects, two different strategies are adopted (displayed in Figure 4). The first strategy is dedicated to the sets of fragments known a priori to be generated by the same event; in this case, the model directly propagates the objects to estimate the epoch of the event. The propagation phase is composed by two steps: the first is the estimation of the date based on the study of the RAAN of each fragment, while the second is the refinement of the first estimate based on the close approach study. Instead, if the set is composed by unknown objects, or by known objects and the goal is to find the origin of a new fragment(s), the model performs a pruning step before the propagation phase. Through this preliminary phase, it is possible to identify and eliminate from the initial set all the fragments that are not related to the ones under consideration (i.e., the new fragments or the ones considered as unknowns). This step is composed by two stages of filtering based on the study of the geometry of the objects' orbit. The output information are the estimated date of the event and a set of fragments probably originated by the event.

3.1 Pruning phase

The pruning phase is composed by two stages: the first is dedicated to the analysis of the inclination of the orbits, while the second compares the geometry of the orbits in terms of distances. The scope of this phase is to filter the initial set of objects such that only the fragments related to the same event arrives at the propagation step.

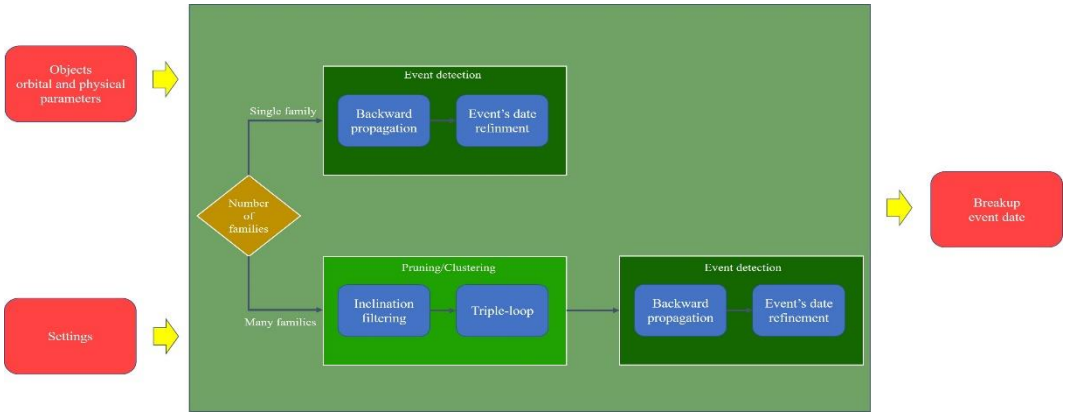

Figure 4. Event detection block diagram.

3.1.1 Inclination filter

The first filtering step is performed considering the inclination as study parameter. In LEO region, the inclination is little affected by perturbations, remaining bounded in time. Consequently, when analysing the origin of a newfound debris, it would be a waste of time to propagate all the orbiting objects to find its origin. Thanks to this property, it is possible to eliminate from the initial set the objects that have the orbit inclination different from the analysed fragment of a certain selected threshold. An example is displayed in Figure 5, where an Iridium 33 debris is considered as unknown (green dot), and it the distribution of other Iridium 33 fragments (in orange) and of other objects (in blue) is studied. As observable, the unknown object is in the same inclination region as the other Iridium 33 fragments. By properly selecting an inclination interval Δi around the green dot, it is possible to reject from the initial set many useless objects while maintaining the correct fragments.

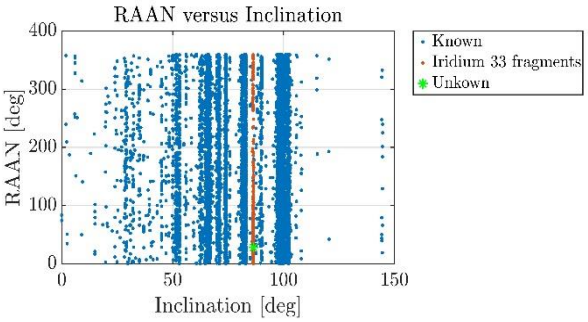

Figure 5a. Location of the unknown object and of the Iridium 33 fragments.

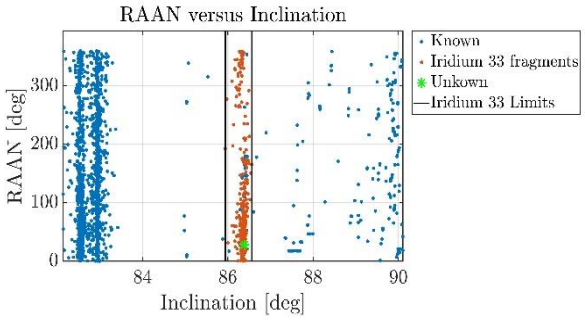

Figure 5b. Iridium 33 limits.

Figure 5. Distribution of the objects in inclination and RAAN

3.1.2 Triple-loop filter

The second filtering step exploits the triple-loop filter, that is composed by three filters: the first two are geometrical comparisons between the orbits, the third is a time filter. The method proposed here was developed by Hoots et al. [4], with a modification in the second filter. The filter compares each time two objects. The first filter examines the apogee and the perigee altitudes of the two analysed objects to check for possible intersections between the orbits. The comparison is performed evaluating the difference between q (defined as the maximum of the two perigee distances) and Q (defined as the minimum of the two apogee distances). In case

$$q - Q \leq D_{th} \qquad (8)$$

where D_{th} is a selected threshold, the object under consideration pass this first filtering stage.

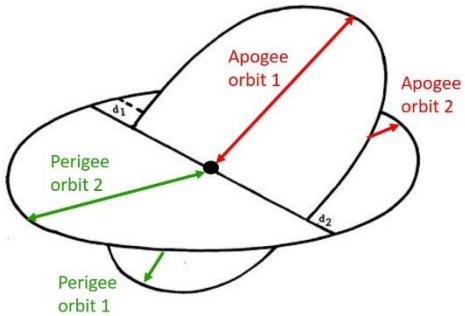

Figure 6. Apogee/Perigee filter: comparison between the apogee and perigee altitudes of the two examined objects' orbits (picture modified from [4]).

The second filter evaluates the MOID between the two orbits to check the possibilities of close approaches. This distance is evaluated using the algebraic method proposed by Gronchi et al. [16] and it is based on the algebraic elimination theory. It computes the roots of a 16^{th} degree univariate polynomial to find the critical points (i.e., minimum, maximum, and saddle points) between the two analysed orbits. Among all the possible solutions, it is selected only the global minimum, and by imposing a second threshold distance, it is possible to eliminate other objects from the initial set. The third filter is based on a time study. Around the MOID points on the first and on the second orbits are generated angular windows (as shown in Figure 7) and it is checked the possibility of finding the analysed objects simultaneously inside these windows considering a fixed time period. In case of cross matches, it is possible that the two objects would presents close encounters. It is important to say that this third filter is not exploited during the pruning phase; this is because away from the event it loses its meaning, while it is extremely useful near the event epoch. For this reason, it is used during the refinement of the date estimation, explained in Section 3.2.3.

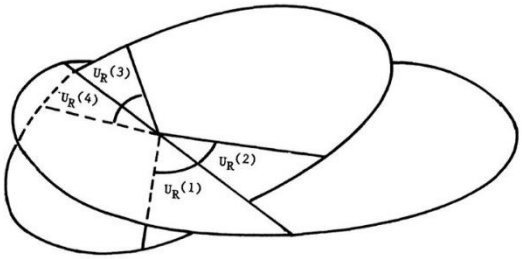

Figure 7. Time filter: check the time of possible close encounters (picture from [4]).

3.2 Event detection

The core of this part of the model is the estimation of the event epoch. In parallel with this, some of the fragments generated by the detected events are also identified as output. The method performs a first estimate analysing the RAAN of the objects, then tries to improve the guess by checking the close encounters between the fragments survived at this point of the process. Since the event epoch is considered as unknown, it is necessary to compute a preliminary guess to set the interval of time within which the propagation is performed. The mid-point of the analysis is evaluated considering a linear variation of the RAAN of each object. Through the propagator, by performing a propagation of a short time period (e.g., one day), are evaluated the parameters needed to build the RAAN lines for each object as

$$\Omega_{new} = \Omega_0 + \dot{\Omega} t \qquad (9)$$

where Ω_0 is the RAAN at the present epoch, and $\dot{\Omega}$ is its actual variation in time. Once all the lines have been defined, the time in which the intersections occur is checked; this epoch is considered as the mid-point of the analysis. The propagation process is performed from the initial date (i.e., the one selected for the investigation) to a final date set as the initial one minus twice the vale obtained from the rough estimate. Then it is performed the real propagation.

3.2.1 Fragments from a single family

In case the initial set is composed by fragments belonging to the same event, the model propagates the objects backward in search of a cluster in the RAAN. Indeed, near the event, this angular parameter is expected to be similar for each fragment. At each time span of the propagation, it is computed a $\Delta\Omega$ evaluated as the difference between the most distant fragments in terms of RAAN. After the propagation reaches the final time, it is detected the time at which the minimum in the $\Delta\Omega$ is found; the latter is the first estimate of the event epoch. Figure 8 shows the evolution in time of $\Delta\Omega$; the example is related to a set of fragments generated during the Cosmos 2251 breakup event. Far from the event, the value of $\Delta\Omega$ is high (in this case, one year after the event it reaches 30 deg), while near the breakup epoch it is identified the minimum value. The time at which the minimum is located is selected as first epoch guess.

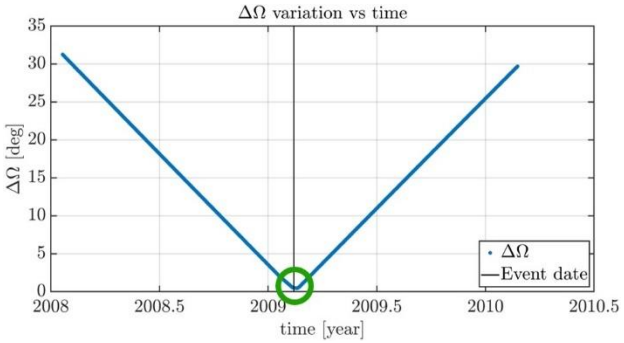

Figure 8. Evolution in time of ΔΩ.

3.2.2 Fragments from different families

After the pruning phase, it is expected that set of the analysed objects is composed of fragments generated by the same parent. However, in some cases it is possible that the filtering stage may not be able to reject all the unwanted fragments. Accordingly, a tool is needed to account for this shortcoming. The basic idea is the same of the single-family case, that is the check in time for a cluster in the RAAN. In addition, a 2D histogram is exploited, whose axis are the sine and the cosine of the RAAN. During the propagation process, it is computed the number of objects in each generated bin and, when the final time of the process is reached, it is searched the epoch at which the bin with the maximum number of objects is located. Close to the event, assuming that the almost totality of the objects included in the set belongs to the same parent, the fragments will be clustered in terms of RAAN generating the maximum bin. Since the possibility of having the maximum bin repeated near the event, among all the possible solutions it is selected the date for which the $\Delta\Omega$ inside the bin is minimum. All the objects that are out of the selected bin are considered as foreign fragments and are eliminated by the process. An example is presented in Figure 9. The figure on the left represents the condition at the beginning of the process, when the fragments involved in the events are spread in RAAN, too. Instead, near the event epoch, the debris belonging to the same family are included in the same bin (the yellow one), while the remaining unwanted objects are out of it.

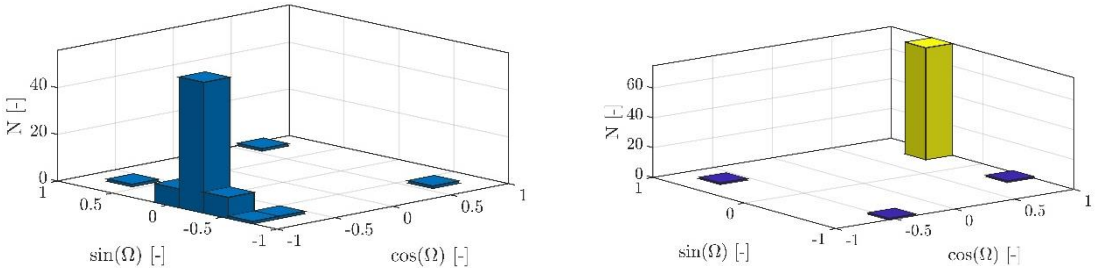

Figure 9. Ω evolution in time, and check of the objects' distribution using a 2D histogram.

3.2.3 Refinement process

The previously evaluated epoch is considered as the first estimate. Then, the model attempts to improve the estimate by examining the close approaches between the studied fragments. For this purpose, the third filter of the triple-loop is exploited; through the method exploited for the filter, it is possible to identify a window of time inside which a close encounter between the two studied fragments is occurred. Then, to find the time of the close encounter, the Newton method is used as in Hoots et al. [4]**.** The iteration is defined as

$$t_{n+1} = t_n - \frac{R_{rel}}{\dot{R}_{rel}} \qquad (10)$$

where t_{n+1} and t_n are the $(n+1)-th$ and the $n-th$ iterations of the process, while R_{rel} and $\dot{R}_{rel}$ are the rate of change of the relative distance between the two objects and its derivative in time, and are evaluated as

$$R_{rel} = r_f \dot{r}_f + r_s \dot{r}_s - \dot{\boldsymbol{r}}_{\boldsymbol{f}} \cdot \boldsymbol{r}_{\boldsymbol{s}} - \boldsymbol{r}_{\boldsymbol{f}} \cdot \dot{\boldsymbol{r}}_{\boldsymbol{s}} \qquad (11)$$

$$\dot{R}_{rel} = \dot{r}^2{}_f + r_f \ddot{r}_f + \dot{r}^2{}_s + r_s \ddot{r}_s - \ddot{\boldsymbol{r}}_{\boldsymbol{f}} \cdot \boldsymbol{r}_{\boldsymbol{s}} - \boldsymbol{r}_{\boldsymbol{f}} \cdot \ddot{\boldsymbol{r}}_{\boldsymbol{s}} - 2\dot{\boldsymbol{r}}_{\boldsymbol{f}} \cdot \dot{\boldsymbol{r}}_{\boldsymbol{s}} \qquad (12)$$

The refinement process is performed by creating a time window around the first epoch guess, inside which the close encounters between each fragment are identified. The, using a histogram, it is evaluated the date at which most of the close encounters are detected; the latter is considered as the second epoch estimate. This kind of analysis is typically carried out considering osculating orbital elements, more suitable to find the precise location in time of the objects. However, since the purpose of this work is to use mean orbital elements, the examination is performed by approximating the osculating orbital elements with the mean one and by checking the performance of the method. The main approximation concerns the osculating mean anomaly approximated by an averaged mean anomaly, because this parameter is fundamental whenever the position of an object on its orbit have to be assessed.

4. Parent identification

The third part of the model is dedicated to the identification of the parent object(s) involved in the event detected in the previous phase. Find the object(s) that are the cause of the event is important to better characterise the breakups (e.g., to model the generated fragments in term of orbital elements). Figure 10 shows the steps of the parent identification model. As for the event detection, this part of the model exploits natural features of the LEO region. The candidates are examined in terms of orbit inclination, are propagated to the estimated event epoch, and finally are checked in terms of orbit geometry and RAAN.

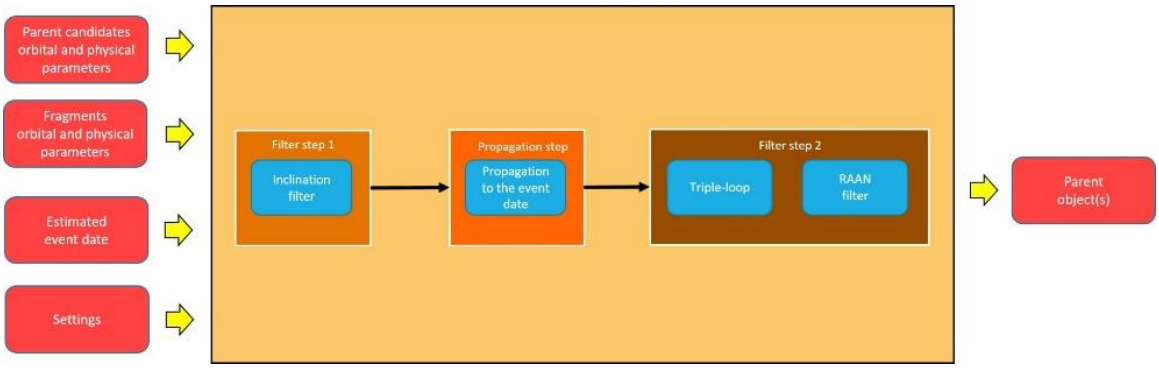

Figure 10. Parent identification block diagram.

4.1 Inclination filter

The first step of the method exploits the inclination to perform the rejection of the wrong candidates. During the event detection phase, in addition to the estimation of the event date, the fragments involved in the event are also found. The idea for this first filtering stage is to compute an average value among the orbit inclination of the analysed fragments. Then, assuming that the objects that generated the debris are near (in terms of inclination) to their fragments, all the candidates that are far from the average value of a certain selected threshold are discarded from the process. As examples are shown the Cosmos 2251 (displayed in Figure 11a) and the Fengyun 1C (displayed in Figure 11b) breakups. The Cosmos fragments are all distributed in a narrow inclination region of about 1 deg around the parent. The Fengyun 1C represents a peculiar case, since the debris are widespread in inclination. However, as observable from the histogram in Figure 12, most of the fragments are located in a small inclination region.

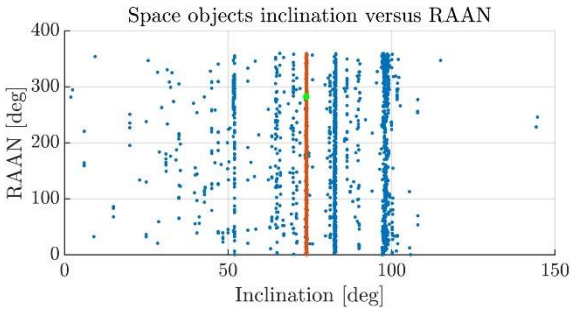

Figure 11a. Cosmos 2251 case.

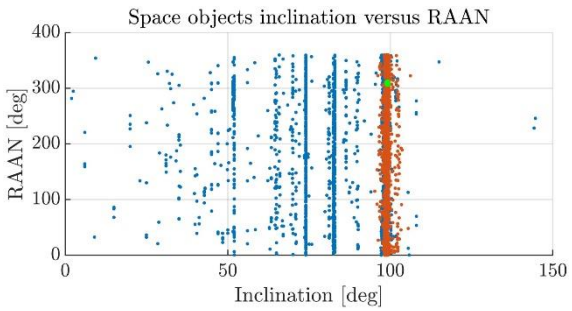

Figure 11b. Fengyun 1C case.

Figure 11. Location of the parent object (in green) with respect its generated fragments (in orange) and other objects (in blue). On the left is presented the Cosmos 2251 case, while on the right the Fengyun case.

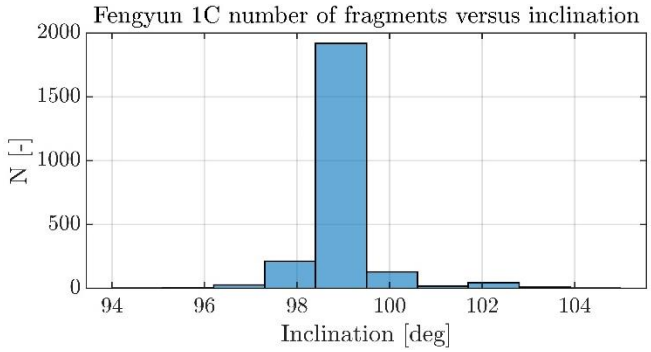

Figure 12. Number of objects per each inclination region - Fengyun 1C.

A possible limitation for this first filtering stage is observed when the parent objects to be found is part of a satellite constellation or family. In these cases, the orbital parameters of the satellites may be similar and hence a high number of objects can move on to the next stages.

4.2 Triple-loop

The second step of the filtering is performed using the geometrical filters of the triple-loop, and it is carried out after the fragments and the candidates are propagated to the estimated event date. As the candidates are propagated near the event epoch, the correct parent and the generated fragments will present similar orbital parameters and will stay close in distance. Consequently, using the triple-loop it is possible to discriminate the candidates included in the set in terms of orbit geometry. As per definition, each candidate is compared with each fragment and, depending on the filter response, two possibilities are considered:

1. Rejection of the candidate in case the filter fails with each fragment;

2. Further study of the candidate in case the filter succeeds for at least one fragment.

Since possible inaccuracies during the propagation phase (mainly related to possible bad estimate of the BC) and since mean orbital elements are considered, the correct candidate may be erroneously eliminated if too stringent values are considered for the thresholds of the two filters. To better visualize the properties of the method, Figure 13 shows the Gabbard plot of a set of candidates (already filtered in inclination and propagated to the event date) and a set of

Cosmos 2251 fragments. The figure represents in blue the perigee altitude and in orange the apogee altitude of each candidate, while the yellow dots are the perigee altitudes, and the purple dots are the apogee altitudes of the fragments. As visible, the objects located at a higher altitude or characterised by a higher orbit period are not compatible with the fragments features and hence must be eliminated by the process.

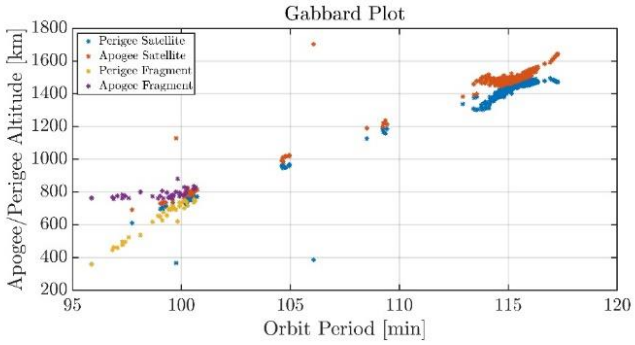

Figure 13. Gabbard plot of fragments and parent candidates.

Figure 14 displays the MOID of each fragment considered in the previous example with the Cosmos 2251 satellite. Almost all values remain below 4 km, while only 2 fragments present a higher value. Using the method proposed, the Cosmos 2251 will not be discarded by the process in case a threshold of 5 km is considered for the MOID filter; contrary, in case the candidate was delated whenever the filter returns negative response for at least one fragment, the correct object would be eliminating by the set.

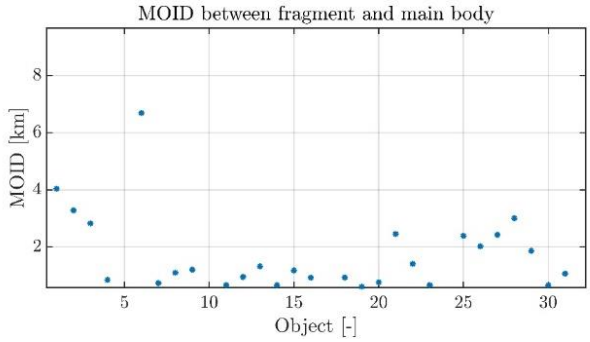

Figure 14. MOID between fragments and Cosmos 2251.

4.3 Right ascension of ascending node

The last step is related to the study of the RAAN of the remaining candidates. Near the event date, the correct parent is expected to have a similar value for this angular orbital parameter to its generated fragments. The methodology adopted is the following:

1. Compute the $\Delta\Omega$ between the fragments and each candidate;
2. Take the minimum values out of all obtained;
3. Reject the candidates exceeding a certain limit.
4. All the candidates that survive after this stage are considerate as equally probable parent(s).

It is important to note that the use of the RAAN is extremely useful when dealing with satellite families. Indeed, near the event date, it is expected that only the correct parent, or however small subset of possible candidate, is close to the fragments in terms of RAAN. An example proposed here is related to the Cosmos 2251 satellite. As observable from the Figure 15, the correct parent (in green) is located near the debris (in blue) in terms of RAAN, while the almost totality of the other candidates (that in this peculiar case are mostly related to the Cosmos family of satellites and are represented in orange) are far from them.

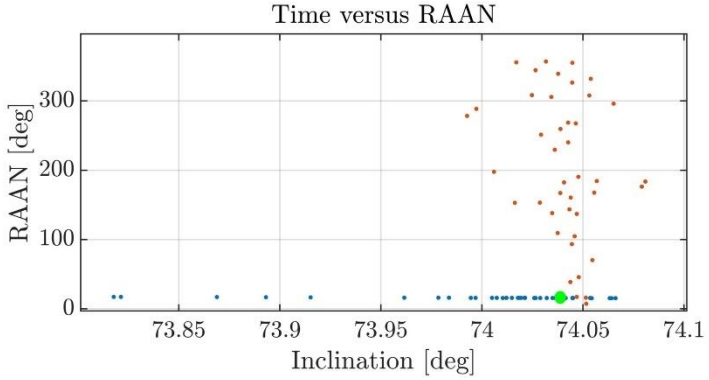

Figure 15. Location of the parent object (in green) in terms of RAAN with respect to its generated fragments (in blue), and other candidates (in orange) - Cosmos 2251.

5. Breakup's scenarios examined

This section examines some known occurred fragmentations used to validate the previously described model. The tests are subdivided according to the composition of the initial sets (i.e., single-family and Fragments from different families test cases). For each set, both the accuracy of the event detection and of the parent identification are assessed. Regarding the event detection method, its validity is checked by evaluating a relative error between the estimated date of the event and real one, computed as

$$\varepsilon_{rell}(\%) = \frac{t_{estim} - t_{real}}{t_{last} - t_{real}} \times 100 \quad (13)$$

where t_{estim} is the estimated date of the event, t_{real} is the real epoch of the event, and t_{last} is the initial time of the analysis. As observable in Eq.13 the error is weighted to the beginning time of the propagation, evaluating the accuracy of the method as the propagation is performed for a higher time span. For the propagation, the following characteristics are considered:

1. Semi-analytic propagator [11];
2. Drag perturbation (with a sinusoidal model for the solar activity evolution in time);
3. Perturbation due to Earth's non spherical gravitational field.

The parent identification routine is investigated by considering different thresholds for each included filter and by searching the edges able to find the correct parent(s). The set of thresholds considered are the following:

1. Inclination Δi: from 0.05 deg up to 5 deg with a step of 0.05 deg;
2. A/P and MOID filters: [5/1, 10/5, 20/10, 40/20, 60/30,80/40, 100/50] km;
3. $\Delta\Omega$ filter: from 0.05 deg up to 5 deg with a step of 0.05 deg.

It is important to state that at this time of the work, it is also acceptable to obtain as final solution for the parent identification a set of possible candidates rather a single candidate.

5.1 Fragments from a single family

Starting from the single-family case, two breakups are considered: the Cosmos 2251 collision breakup occurred on 10 February 2009 [17] (during a minimum in the solar activity), and the NOAA 16 breakup (assessed to be an explosion [17]) occurred on 25 November 2015 [17] (during a period of higher solar activity). The scope is to observe the behaviour of the method as function of the initial date and of the characteristics of the initial date. The initial set of objects are composed by 51 objects for the Cosmos 2251 case, while 61 objects for the NOAA 16 case.

5.1.1 Event detection

The examination is performed considering the initial date for the analysis at 1, 6, 12, 18, 24, and 30 months after each breakup epoch. For each test case is evaluated the relative error for the first epoch estimate, while the refinement technique is applied to the 1-, 6-, and 12-months cases. Figure 16 shows the relative errors evaluated as function of the initial date. In both cases small errors are obtained, but the Cosmos 2251 case presents a better behaviour as the propagation is performed for a longer time span with respect to the NOAA 16 tests. This result may be associated to three different possible problems: the inaccuracy of a simple sinusoidal model to recover the solar activity evolution (mainly for higher solar activity periods), the possible poor accuracy in the BC estimation of some fragments, or possible inaccuracy in the propagator itself. As observable in Figure 17, the minimum $\Delta\Omega$ increases as well, and it is probably directly correlated to the possible higher error in the epoch estimation.

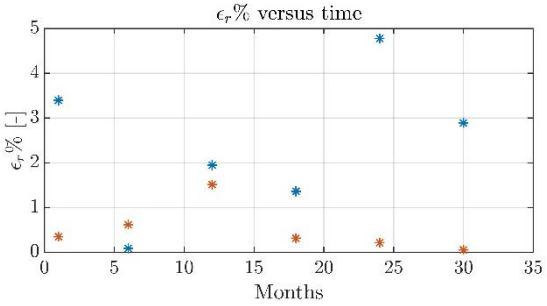

Figure 16. Relative error of the first epoch estimates as function of the initial date; Cosmos 2251 errors are in orange, while NOAA 16 errors are in blue.

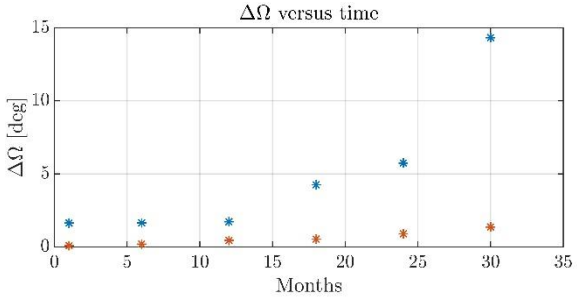

Figure 17. $\Delta\Omega$ at the event epoch as function of the initial date. Cosmos 2251 results in orange, while NOAA 16 results in blue.

Looking at the performances of the refinement technique, Figure 18 shows that no improvements are achieved for the Cosmos 2251 tests (however already characterised by a very low error); instead, shows an improvement in the result for the 1-month case, while a worsening in the result for the 12-months case. The source of this error can be associated to a loss in the accuracy of the hypothesis made to perform this analysis. Indeed, looking at Figure 20 and Figure 21, that display the number of detected close encounter as function of time around the first epoch estimate, it is possible to observe that the bins around the maximum one tends to increase the number of elements, reducing the precision of the entire process.

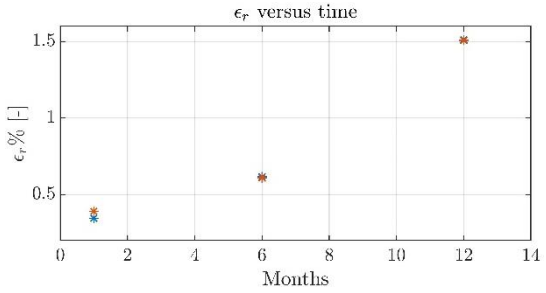

Figure 18. Cosmos 2251 comparison between the first estimate relative error and the second estimate relative error.

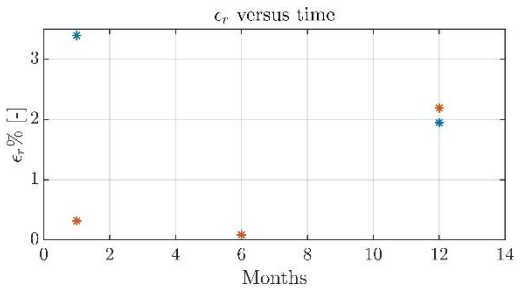

Figure 19. NOAA 16 comparison between the first estimate relative error and the second estimate relative error.

Another source of error could be the increment in the $\Delta\Omega$, that can be related to a wrong estimation of the MOID point and hence of the window generated around them to detect the close encounters.

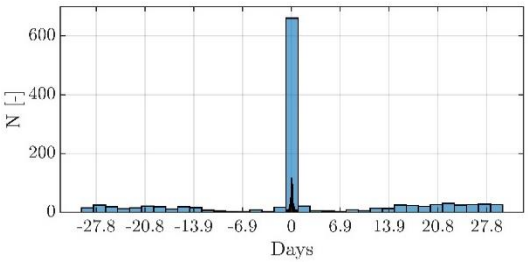

Figure 20. Number of close encounters per each day from the first epoch estimate - 1-month case.

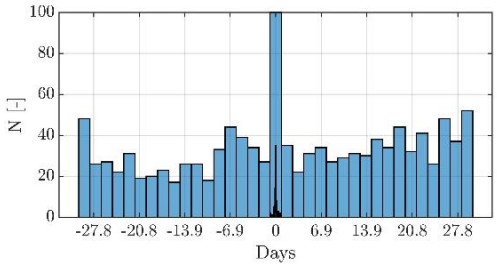

Figure 21. Number of close encounters per each day from the first epoch estimate - 12-months case.

5.1.2 Parent identification

The same sets are exploited for the identification of the parent(s). First it is checked the efficacy of the inclination filter, performed before all the objects are propagated at the estimated event epoch. Then, for the second part of the filtering are tested the results obtained considering a Δi equal to 0.5 deg for the first filtering threshold. Figure 22 and Table 1 summarise the results for the Cosmos 2251. The inclination filter can eliminate many objects, especially if stringent values for the threshold are adopted, while always including the correct parent in the final set. However, many candidates remain after this filter stage, and the reason is that the Cosmos 2251 belongs to a satellites' family; consequently, many Cosmos satellites that present a similar value for the inclination parameter are not rejected by the process. Instead, looking at the final results in Table 1, it is possible to state that the method is able to find the correct parent by properly choosing the thresholds for each step.

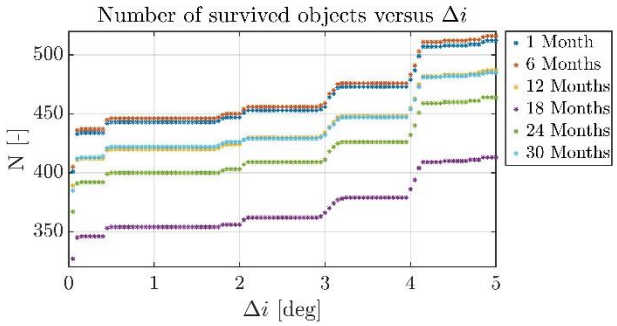

Figure 22. Number of survived fragments after the inclination filtering stage - Cosmos 2251.

	1	6	12	18	24	30
# Initial candidates	1719	1777	1673	1486	1678	1703
Single Candidate	Yes	Yes	Yes	Yes	Yes	Yes
A/P - MOID (km)	5-1	5-1	5-1	5-1	5-1	5-1
$\Delta\Omega$ (deg)	0.05	0.05	0.4	0.1	0.15	0.15
# Multiple Candidates	-	-	-	-	-	-
A/P - MOID (km)	-	-	-	-	-	-
$\Delta\Omega$ (deg)	-	-	-	-	-	-

Table 1. Results for the parent identification - Cosmos 2251 case.

Regarding the NOAA 16 case, Figure 23 shows that the inclination filter performances are more powerful when the threshold is set below 2 deg. However, in these test cases, the model is not able to include the correct candidate if the inclination threshold is set at 0.05 deg (very stringent value) and the initial time for the propagation goes far from the event one. Looking at the Table 2, this time the model is able to find the correct parent for the 1- and 6-months cases, while for longer period the method is able to narrow the final set of candidates to a smaller one (at maximum 5 final candidates, starting from a set of 2689 initial candidates).

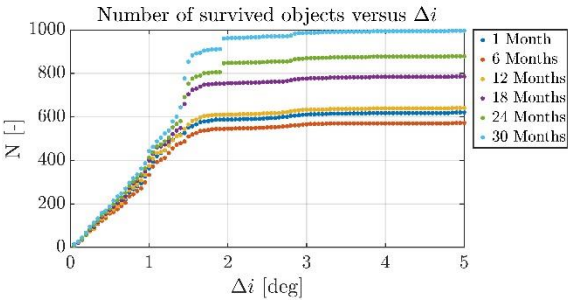

Figure 23. Number of survived fragments after the inclination filtering stage - NOAA 16 case.

	1	6	12	18	24	30
# Initial candidates	2104	1888	2090	2242	2360	2689
Single Candidate	Yes	Yes	No	No	No	No
A/P - MOID (km)	5-1	5-1	-	-	-	-
ΔΩ (deg)	1	0.1	-	-	-	-
# Candidates	-	-	2	3	2	5
A/P - MOID (km)	-	-	5-1	5-1	5-1	5-1
ΔΩ (deg)	-	-	0.65	1.45	2.5	3.85

Table 2. Results for the parent identification - NOAA 16 case.

5.2 Fragments from different families

The tests for the set composed by objects generated by different events is carried out by randomly composing the initial set and by adding fragments belonging to a chosen family, that is the one under analysis. Here are presented two cases, considering the breakups of the Iridium 33 and the Fengyun 1C. For each breakup are considered three different test cases, changing each time the debris initially considered as unknown. The scope is to observe the sensitivity of the model to different initial unknowns.

5.2.1 Iridium 33

The initial data for the process are dated 11 May 2009 and the initial set considered is composed by 360 objects, of which 79 are Iridium 33 fragments. The epoch of the breakup event is considered as 11 February 2009 [17]. Before the propagation process, the initial set is analysed through the pruning phase, and the results for each considered unknown objects is summarised in Table 3. In each case, the model rejects the undesired fragments, leaving in the study set only fragments belonging to the correct event.

	34594	34522	34494
# Total Objects	31	22	11
# Iridium 33 Fragments	31	22	11

Table 3. Number of objects after the pruning phase - Iridium 33 case.

The remaining objects are then propagated, and Figure 24 are compared the results obtained with the first and the refined estimates. For the first and the third test cases, the model is able to improve the initial epoch guess, while for the second case there is a worsening in the final result. Regarding the parent identification, the initial set of candidates is composed by 1577 objects. Figure 25 shows the trend in the number of objects included in the set after the inclination filter. All the thresholds can include the correct candidate, unless for the third study case for which the selection of a Δi equal to 0.05 deg fails. However, the latter is a very stringent threshold value. Moreover, it is possible to observe a high improvement in the filtering when threshold lower than 4 deg are selected. For the second step are selected the candidates survived from the inclination filter when selecting a Δi equal to 0.5 deg. Table 4 reports the final results; the model is not able to find the correct parent, but the number of final candidates decreases if compared to the initial one, with at maximum 9 objects included in the final set.

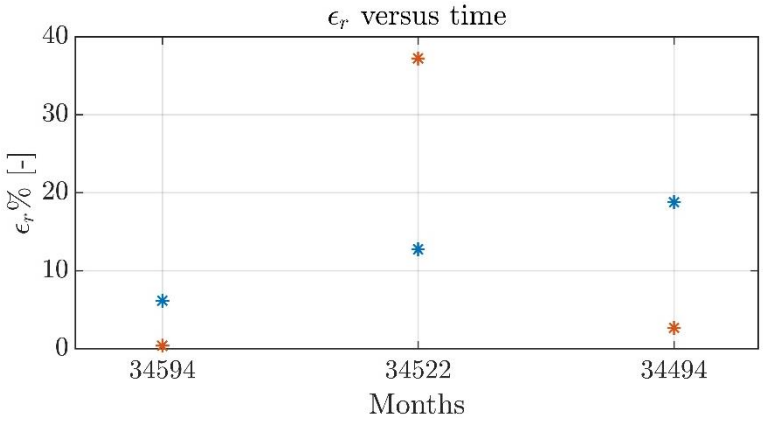

Figure 24. Iridium 33 comparison between the first estimate error and the second estimate error as function of the initial unknown object.

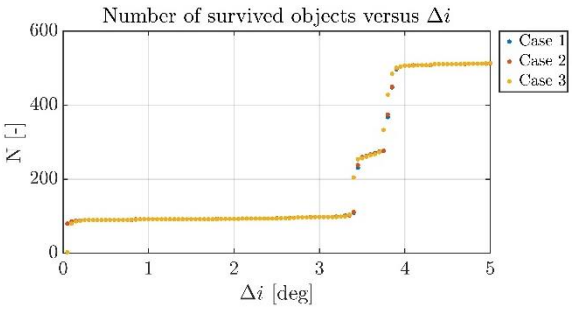

Figure 25. Number of survived fragments after the inclination filtering stage - Iridium 33 case.

	34594	34522	34494
Single Candidate	No	No	No
A/P - MOID (km)	-	-	-
$\Delta\Omega$ (deg)	-	-	-
# Multiple Candidates	5	8	9
A/P - MOID (km)	5-1	5-1	10-5
$\Delta\Omega$ (deg)	0.2	0.5	0.45

Table 4. Results for the parent identification - Iridium 33 case.

5.2.2 Fengyun 1C

The initial set of analysed objects is composed by 405 objects, of which 72 are Fengyun 1C fragments. The initial data are dated 10 November 2007, while the breakup events occurred on 10 January 2007 [17], hence ten months before the beginning time for the analysis. As before, three different debris are considered as unknown objects and the pruning phase is performed per each test case. The results are reported in following table.

	29780	29729	29765
# Total Objects	12	25	15
# Fengyun 1C Fragments	12	21	15

Table 5. Number of objects after the pruning phase - Fengyun 1C case.

In this case, for the second test case, the model is not able to include in the final set fragments belonging to the Fengyun only, but 4 foreign objects remain in the process. This cand be related to the location of the occurred event. Indeed, the Fengyun 1C breakup has occurred in a region denser of objects; this inevitably increases the complexity of the pruning phase.

Figure 26 displays the results of the propagation phase. As observable, the refinement technique fails each time, producing worse result for the second estimate. Probably the reasons are associated to the low number of objects available at the refinement process for the close encounters detection, and to the time span considered for the analysis, that could be too long for the validity of the hypothesis performed.

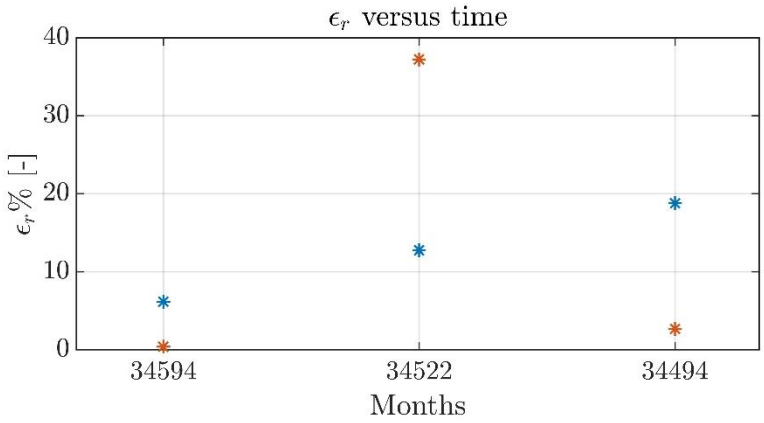

Figure 26. Fengyun 1C comparison between the first estimate error and the second estimate error as function of the initial unknown object.

Regarding the parent identification, the initial set of possible candidates is composed by 1497 objects. Figure **27** shows the trend of survived candidates as function of the inclination threshold, while Table 6 reports the final results (considering a threshold of 0.5 deg for the inclination filter). This time, only for the second test case it is not possible to identify the correct parent; however, the final set is composed by only two objects.

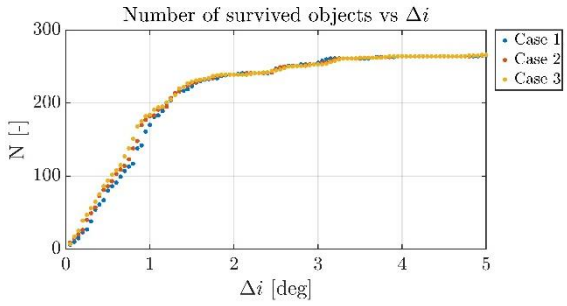

Figure 27. Number of survived fragments after the inclination filtering stage - Fengyun 1C case.

	34594	34522	34494
Single Candidate	No	No	No
A/P - MOID (km)	-	-	-
$\Delta\Omega$ (deg)	-	-	-
# Multiple Candidates	5	8	9
A/P - MOID (km)	5-1	5-1	10-5
$\Delta\Omega$ (deg)	0.2	0.5	0.45

Table 6. Results for the parent identification - Fengyun 1C case.

6. Conclusions

The main objectives of the proposed work were the localisation of possible occurred fragmentations and the identification of the object(s) that generated the fragments. The use of mean orbital elements and of a time span of the order of months up to years to study the evolution in time of the objects motion makes analysis more challenging than considering a short time span. The paper describes in detail each model and each method adopted to fulfil the goals. The entire model developed exploits LEO's natural properties (e.g., the little influence of the perturbation over the orbit inclination) to build methods useful for both the detection of the event and the identification of the parent(s). As clearly observable, there are similarities between the first and the second part of the model since the feature to be analysed are the same. Indeed, the orbit inclination and RAAN are extremely important features, with the first powerful also far from the event date, while the second becomes dominant near the event. The use of pruning and clustering techniques is essential to reject from the process all the objects not desired and to avoid the propagation of a too large number of objects. Looking at the tests proposed, the method shows accuracy for both the event detection and the parent identification routines. The latter is also able, in some cases, to find the correct parent, while in general to reduce the number of candidates to a small set.

Some limitation to the model were encountered during the validation phase. First, the possible inaccuracy in the BC estimation, especially for objects characterised by a high area-to-mass ratio; the latter are highly influenced by the drag and hence by the solar activity cycles. The idea is to improve the accuracy by fitting the BC estimate and to compare the results with real data. The examinations highlight the need of new pruning/clustering algorithms to manage unknown fragments located in space regions denser of objects. The refinement technique seems to work properly for some cases, while for other it fails. Consequently, the idea is to introduce osculating orbital elements to perform short term analyses near the breakup events, maintaining the use of the mean orbital elements for the first estimation of the date. Lastly, the propagator is currently a bottleneck for the number of objects that can be included in the initial set of the study; a high number of objects parallel to a high accuracy slow down the process.

In addition to the previously cited improvements, the idea is to implement the entire model into a software suite to expand the research window of the software PUZZLE [3], which focuses on short term analyses. Moreover, the idea is to further expand the model with two additional routines: on the one hand to consider other space regions (e.g., GEO, MEO, HEO) and their possible interaction to have a mor global knowledge of the space around the Earth, on the other hand the modelling in space of the fragments generated by the events would be useful to perform collision risk analyses suitable to understand the influence of the breakup events on the objects around it.

Acknowledgements

This research has received funding as part of the COMPASS project: "Control for orbit manoeuvring by surfing through orbit perturbations". (Grant agreement No 679086). This project is European Research Council (ERC) funded project under the European Union's Horizon 2020 research.

References

[1] ESA Space Debris Office, "ESA's Annual Space Environment Report," 2020. [Online]. Available: https://www.sdo.esoc.esa.int/environment_report/Space_Environment_Report_latest.pdf.

[2] R. L. Andrisan, A. G. Ionita, R. D. Gonzàlez, N. Ortiz and H. Krag, "Fragmentation Events analysis Making use of fragmentation model and Assessment Tool (FREMAT)," in *7th European Conference on Space Derbis*, Darmstadt, Germany, Apr. 17-21 2017.

[3] M. Romano, A. Muciaccia, M. Trisolini, P. Di Lizia, C. Colombo, A. Di Cecco and L. Salotti, "PUZZLE software for the characterisation of in-orbit fragmentations," in *8th European Conference on Space Debris*, Darmstadt, Germany, Virtual Conference, Apr. 20-23 2021.

[4] F. R. Hoots, L. L. Crawford and R. L. Roehrich, "An analytic method to determine future close approaches between satellites," *Celestial Mechanics,* vol. 33, pp. 143-158, 1984.

[5] V. Zappala, C. A., F. P. and Z. Knezevic, "Asteroid families. identification by hierarchical clustering and reliability assessment," *The Astronomical Journal,* p. 100:2030–2046, 1990.

[6] L. Dimare, S. Cicalò, A. Rossi, E. M. Alessi and G. Valsecchi, "In-Orbit Fragmentation Characterization and Parent Bodies Identification by Means of Orbital Distances," in *1st International Orbital Debris Conference (IOC),* Sugarland, Houston, TX, USA, Dec. 9-12 2019.

[7] R. B. Southworth and G. S. Hawkins, "Statistics of Meteor Streams," *Smithsonian Contributions to Astrophysics,* vol. 7, pp. 261-285, 1963.

[8] T. Jopek, "Remarks on the Meteor Orbital Similarity D-Criterion," *Icarus,* vol. 106, pp. 603-607, Dec. 1993.

[9] J. D. Drummond, "A test of comet and meteor shower associations," *Icarus,* vol. 45, pp. 545-553, Mar. 1981.

[10] S. Frey, C. Colombo and S. Lemmens, "Density based modelling and indication of break-up location and epoch from fragments using backwards propagation," in *5th European Workshop on Space Debris Modelling and Remediation,*, Paris, France, Jun. 25-27 2018.

[11] C. Colombo, "Planetary orbital dynamics (PlanODyn) suite for long term propagation in perturbed environment," in *Proceedings of the 6th International Conference on Astrodynamics Tools and Techniques (ICATT)*, Darmstadt, Germany, Mar. 2016.

[12] A. Lidtke, D. Gondelach and R. Armellin, "Optimising filtering of two-line element sets to increase re-entry prediction accuracy for GTO objects," *Advances in Space Research,* vol. 63, pp. 1289-1317, Feb. 2019.

[13] D. Gondelach, R. Armellin and A. Lidtke, *Mathematical Problems in Engineering,* Nov. 2017.

[14] S. Frey, C. Colombo, D. Gondelach and R. Armellin, "Extension of the King-Hele orbital contraction method and application to the geostationary transfer orbit re-entry prediction," in *4th International Workshop on Space Debris Re-entry,* ESOC, Darmstadt, 28 Feb. 2018.

[15] D. Vallado, P. Crawford, R. Hujsak and T. Kelso, "Revisiting spacetrack report no. 3: Rev. 1," 2006.

[16] G. F. Gronchi, "An algebraic method to compute the critical points of the distance function between two keplerian orbits," *Celest. Mech. Dyn. Astron,* vol. 93 , pp. 295-329, 2005.

[17] P. D. Anz-Meador, J. N. Opiela, D. Shoots and J.-C. Liou, "History of On-orbit satellite fragmentations 15th Edition," 2018. [Online]. Available: https://ntrs.nasa.gov/api/citations/20180008451/downloads/20180008451.pdf..